



HAL
open science

Ferromagnetic resonance and magnetic damping in C-doped Mn₅Ge₃

Charles Emmanuel Dutoit, Voicu Dolocan, Michael Kuzmin, Lisa Michez,
Matthieu Petit, Vinh Le Thanh, Benjamin Pigeau, Sylvain Bertina

► **To cite this version:**

Charles Emmanuel Dutoit, Voicu Dolocan, Michael Kuzmin, Lisa Michez, Matthieu Petit, et al..
Ferromagnetic resonance and magnetic damping in C-doped Mn₅Ge₃. *Journal of Physics D: Applied
Physics*, 2015, 49 (4), pp.045001. 10.1088/0022-3727/49/4/045001 . hal-01266713

HAL Id: hal-01266713

<https://amu.hal.science/hal-01266713v1>

Submitted on 19 Jul 2016

HAL is a multi-disciplinary open access archive for the deposit and dissemination of scientific research documents, whether they are published or not. The documents may come from teaching and research institutions in France or abroad, or from public or private research centers.

L'archive ouverte pluridisciplinaire **HAL**, est destinée au dépôt et à la diffusion de documents scientifiques de niveau recherche, publiés ou non, émanant des établissements d'enseignement et de recherche français ou étrangers, des laboratoires publics ou privés.

Ferromagnetic resonance and magnetic damping in C-doped Mn_5Ge_3

(Dated: May 15, 2015)

X-band ferromagnetic resonance (FMR) was used to investigate static and dynamic magnetic properties of Mn_5Ge_3 and Carbon-doped Mn_5Ge_3 ($\text{C}_{0.1}$ and $\text{C}_{0.2}$) thin films grown on Ge(111). The temperature dependence of magnetic anisotropy shows an increased perpendicular magneto-crystalline contribution at low temperature with an in-plane easy axis due to the large shape contribution. We find that our samples show as small as 40Oe FMR linewidth (corresponding Gilbert damping $\alpha=0.005$), for the out-of-plane direction, certifying of their very good structural quality. The perpendicular linewidth shows a minimum around 200K for all samples, which seems not correlated to the C-doping. The magnetic relaxation parameters have been determined and indicate as main extrinsic contribution the two-magnon scattering. A transition from six-fold to two-fold plus fourth-fold in-plane anisotropy is observed in the FMR linewidth of $\text{Mn}_5\text{Ge}_3\text{C}_{0.2}$ around 200K.

I. INTRODUCTION

The field of semiconductor spintronics is rapidly developing nowadays. The idea to combine the well established data processing capabilities of semiconductor electronics with ferromagnetism may lead to new functionalities and low power consumption of devices^{1,2}. One of the main obstacle for spin injection into a semiconductor is the conductivity mismatch at the interface of the ferromagnetic metal and the semiconductor³. One way to avoid it is to use a thin insulating layer acting as a tunnel barrier between the two materials. Another approach is to design the spin injecting interface with a similar structure and properties by alloying or doping the semiconductor with a magnetic element.

The intermetallic magnetic Mn_5Ge_3 could provide the desired solution as it grows directly onto Ge substrate⁴, therefore being compatible with existing semiconductor technology. Mn_5Ge_3 shows ferromagnetism with a Curie temperature (T_c) around room temperature⁵ and an important spin polarization (up to 42%)^{6,7}. The Mn_5Ge_3 hexagonal cell contains 10 Mn atoms which are arranged in two different sublattices (Mn_I and Mn_{II}) due to different coordination. Inserting Carbon atoms into interstitial voids of Mn_{II} octahedra leads to an increase of T_c up to 450K, supplying a solution for the room temperature spin injection⁸. *Ab-initio* calculations indicate that the structural distortions have a small influence on the increased T_c in $\text{Mn}_5\text{Ge}_3\text{C}_x$ (the lattice is compressed compared to pure Mn_5Ge_3), with the enhanced ferromagnetism attributed to a 90° ferromagnetic superexchange mediated by Carbon⁹.

Several preparation methods were used to grow Mn_5Ge_3 thin films. The most common growth method is the solid phase epitaxy which consists in the deposition of Mn or Mn and C on a Ge(111) layer followed by an annealing leading to the formation of the Mn_5Ge_3 or $\text{Mn}_5\text{Ge}_3\text{C}_x$ films. Due to the low Mn solubility in Ge, secondary precipitates or Mn-rich regions/clusters frequently appear inside the Mn_5Ge_3 films. Mn atoms also diffuse in the underlying Ge(111) substrate which deteriorates the interface quality. In this letter, we report on the structural and magnetic properties of thin films C-doped Mn_5Ge_3 epitaxially grown on Ge(111) by reactive deposition epitaxy (RDE) at room temperature.

The low growth temperature reduces segregation and allows the formation of thin films of excellent crystalline quality suitable for the determination of various magnetic parameters by FMR: magnetic anisotropy, magnetization and the g -factor which were quantitatively determined and their dependence on Carbon content and temperature was identified. From the study of the FMR linewidth, the magnetic relaxation process is investigated and the relaxation parameters are found. The main relaxation channels we identify are the intrinsic Gilbert damping and the two-magnon scattering. The ferromagnetic resonance measurements demonstrate the very good structural quality of the pure and C-doped Mn_5Ge_3 , paving the way for heterostructures integration.

II. EXPERIMENTAL DETAILS

The sample preparation as well as the reflection high-energy electron diffraction (RHEED) measurements were performed in a UHV setup with a base pressure of 2.7×10^{-8} Pa. $\text{Mn}_5\text{Ge}_3\text{C}_x$ layers were grown epitaxially on Ge(111) substrates^{4,10}. These substrates were chemically cleaned before introduction in the UHV chamber. Then we did a degassing of the Ge(111) substrates by direct heating up to 720 K for 12 h and flashed afterwards at 1020 K to remove the native oxide layer. After repeated flashes at 1020 K and a cooling down at 770 K, a 15 nm thick Ge buffer layer was deposited on the Ge(111) substrates to make sure that the starting surface of the $\text{Mn}_5\text{Ge}_3\text{C}_x$ thin films growth is of good quality. The quality of this starting surface was checked *in-situ* by RHEED. Eventually the sample was cooled down to room temperature (RT).

To form the $\text{Mn}_5\text{Ge}_3\text{C}_x$ layers we used the reactive deposition epitaxy method¹¹. Using this method the $\text{Mn}_5\text{Ge}_3\text{C}_x$ layers are created by phase nucleation at the surface of the sample during the epitaxial growth. No diffusion phenomenon is required for the growth unlike the solid phase epitaxy process which is usually employed to form the $\text{Mn}_5\text{Ge}_3\text{C}_x$ films on Ge(111). However a good control of the different flows is needed to match the stoichiometry of the desired compound : Ge and Mn were evaporated using Knudsen cells and C atomic flow was obtained thanks to a high purity pyrolytic graphite fila-

89 ment source (SUKO) from MBE-Komponenten. The Ge
 90 and Mn flows were calibrated with a water-cooled quartz
 91 crystal microbalance and the C flow was calibrated using
 92 the structure transition between the Si(001) (2×1) and
 93 $c(4\times 4)$ reconstructions which occurs for a C deposited
 94 thickness of 0.4 atomic monolayer on Si(001) surfaces¹².
 95 The growth of the $\text{Mn}_5\text{Ge}_3\text{C}_x$ films was monitored *in-*
 96 *situ* by RHEED : the $\text{Mn}_5\text{Ge}_3\text{C}_x$ films growing epitaxially
 97 on a Ge(111) surface exhibit an easily identifiable
 98 RHEED ($\sqrt{3}\times\sqrt{3}$)R30° pattern which is characteristic
 99 of the Mn_5Ge_3 and $\text{Mn}_5\text{Ge}_3\text{C}_x$ compounds^{10,13}.

100 The saturation magnetization and the estimated Curie
 101 temperatures of all samples were determined by SQUID
 102 measurements. A SQUID magnetometer Quantum De-
 103 sign MPMSXL working in a temperature range 1.8K to
 104 300K and in a magnetic field up to 5T was used. The
 105 FMR measurements were performed with a conventional
 106 X-band (9.39GHz) Bruker EMX spectrometer in the 80K
 107 to 300K temperature range. The samples ($2\times 2\text{mm}^2$)
 108 were glued on quartz suprazil rode and mounted in the
 109 center of a rectangular cavity (TE_{102}). To improve the
 110 signal-to-noise ratio, the FMR measurements are carried
 111 out using a modulation field of 100kHz and 50e amplitude
 112 with a lock-in detection. The FMR spectra were
 113 measured with the applied magnetic field rotated in plane
 114 and out-of-plane. The FMR spectra were fitted with a
 115 Lorentzian profile and the resonance field and FWHM
 116 linewidth were subsequently extracted. Typical spectra
 117 at room temperature are shown in Fig. 1(a) for thin films
 118 of 12nm thickness.

119 III. MODEL AND GEOMETRY

120 The FMR spectra were analyzed with the Smit-Beljers
 121 formalism for a thin film with uniaxial (hexagonal)
 122 symmetry¹⁴. For a ferromagnetic film with hexagonal
 123 symmetry, the free energy density including the Zeeman
 124 energy, the demagnetizing energy and the anisotropy en-
 125 ergy density is written as:

$$F = -MH[\sin\theta\sin\theta_H\cos(\varphi-\varphi_H) + \cos\theta\cos\theta_H] \\ - (2\pi M^2 - K_2)\sin^2\theta + K_4\sin^4\theta + K_{6\perp}\sin^6\theta \\ + K_{6\parallel}\sin^6\theta\cos 6\varphi \quad (1)$$

126 where θ_H , φ_H are the polar and azimuthal angle of the
 127 external field with respect to the surface normal of the
 128 thin film ([001] direction) and respectively [100] direction,
 129 θ and φ are the polar and azimuthal angle of the magneti-
 130 zation with respect same directions (Fig. 1(b)) and K_i are
 131 the anisotropy constants to sixth order. The resonance
 132 condition, neglecting the damping effects and consider-
 133 ing the magnetization at equilibrium under steady field,
 134 is given by:

$$\left(\frac{\omega}{\gamma}\right)^2 = H_1 \cdot H_2 \quad (2)$$

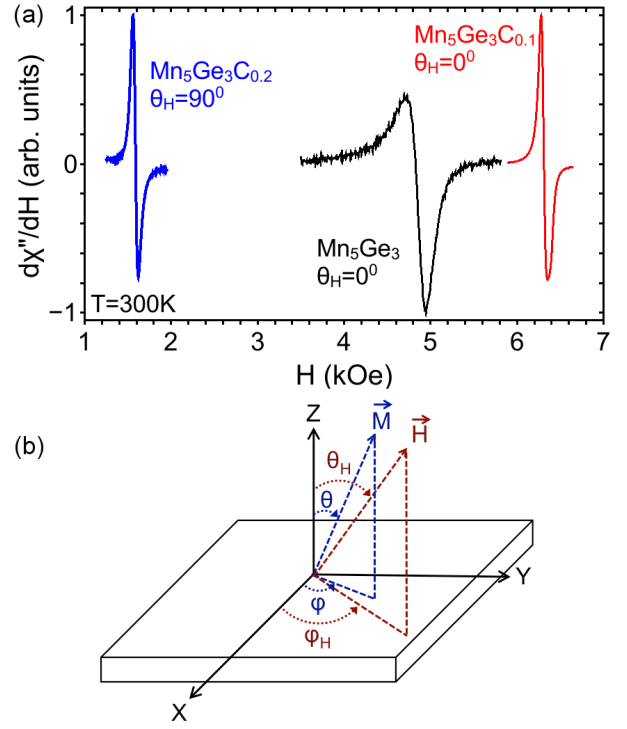


FIG. 1. (Color online) (a) Typical spectra at room temper-
 ature for Mn_5Ge_3 , $\text{Mn}_5\text{Ge}_3\text{C}_{0.1}$ and $\text{Mn}_5\text{Ge}_3\text{C}_{0.2}$ thin films
 with 12nm thickness. (b) Schema of the coordinate system
 used in FMR measurements.

135 where H_1 and H_2 represent the stiffness fields evaluated
 136 at the equilibrium angles of the magnetization:

$$H_1 = \frac{1}{M} \frac{\partial^2 F}{\partial \theta^2} \quad (3)$$

$$H_2 = \frac{1}{M \sin^2 \theta} \frac{\partial^2 F}{\partial \varphi^2} \quad (4)$$

137 Equation (2) is valid for a high-symmetry case, where
 138 the mixed second derivative of the free energy is nil. Our
 139 experiments were carried out in two distinct geometries:

(i) out-of-plane geometry ($\varphi_H = 0^\circ$, θ_H variable). The
 stiffness fields are the following:

$$H_1^\perp = H_r \cos(\theta - \theta_H) - 4\pi M_{eff} \cos 2\theta + 2\frac{K_4}{M}(\cos 2\theta \\ - \cos 4\theta) + 30\frac{(K_{6\perp} + K_{6\parallel})}{M} \sin^4 \theta \\ - 36\frac{(K_{6\perp} + K_{6\parallel})}{M} \sin^6 \theta \quad (5)$$

$$H_2^\perp = H_r \cos(\theta - \theta_H) - 4\pi M_{eff} \cos^2 \theta + 4\frac{K_4}{M}(\cos^2 \theta \\ - \cos^4 \theta) + 6\frac{(K_{6\perp} + K_{6\parallel})}{M} \sin^4 \theta \cos^2 \theta - 36\frac{K_{6\parallel}}{M} \sin^6 \theta \quad (6)$$

140 (ii) in-plane geometry ($\theta_H = 90^\circ$, φ_H variable). The
141 stiffness fields are:

$$H_1^\parallel = H_r \cos(\varphi - \varphi_H) + 4\pi M_{eff} - 4\frac{K_4}{M} - 6\frac{K_{6\perp}}{M} - 6\frac{K_{6\parallel}}{M} \cos 6\varphi \quad (7)$$

$$H_2^\parallel = H_r \cos(\varphi - \varphi_H) - 36\frac{K_{6\parallel}}{M} \cos 6\varphi \quad (8)$$

142 Here $4\pi M_{eff} = 4\pi M - \frac{2K_2}{M}$, ω the angular frequency
143 and $\gamma = g\mu_B/\hbar$ the gyromagnetic ratio. $H_{1,2}^\perp$ represent
144 the stiffness fields for the out-of-plane geometry ($\theta_H = 0$)
145 and $H_{1,2}^\parallel$ for the in-plane geometry ($\theta_H = 90^\circ$).

146 The FMR linewidth is analyzed by including the in-
147 trinsic and extrinsic damping mechanisms¹⁵⁻¹⁷ :

$$\Delta H = \Delta H_{intr} + \Delta H_{extr} \quad (9)$$

148 In this expression, the intrinsic contribution due to the
149 magnon-electron interaction can be described by the di-
150 mensionless Gilbert damping parameter α ^{18,19}:

$$\Delta H_{intr} = \frac{2\alpha\omega}{\gamma\Psi} \quad (10)$$

151 where $\Psi = \frac{1}{H_1 + H_2} \frac{d(\omega^2/\gamma^2)}{dH_r}$ is the dragging function as
152 the magnetization \mathbf{M} is dragged behind \mathbf{H} owing to
153 anisotropy. When \mathbf{M} and \mathbf{H} are parallel, this contribu-
154 tion vanishes. As generally the in-plane and out-of-plane
155 linewidth are not equal, extrinsic contribution have to
156 be taken into account. The extrinsic contribution gener-
157 ally include the magnetic relation due to magnon-magnon
158 interaction, the two-magnon interaction, which is given
159 by²⁰⁻²³:

$$\Delta H_{2mag} = \frac{\Gamma}{\Psi} \quad (11)$$

160 with Γ the two-magnon scattering rate. The two-magnon
161 contribution usually vanishes for a critical out-of-plane
162 angle $\theta < 45^\circ$. Inhomogeneous broadening effects also
163 participate to the extrinsic linewidth, especially at in-
164 termediate angles as the resonance local field can vary.
165 We consider here three types of inhomogeneous broad-
166 ening: ΔH_{mos} , ΔH_{int} and ΔH_{inhom} . The first term is
167 the mosaicity term due to the distribution of easy axes
168 directions^{15,19}:

$$\Delta H_{mos} = \left| \frac{\partial H_r}{\partial \beta_H} \right| \Delta \beta_H \quad (12)$$

169 with $\beta_H = (\theta_H, \varphi_H)$. The second term represents the
170 inhomogeneity of the internal fields in the sample¹⁷:

$$\Delta H_{int} = \left| \frac{\partial H_r}{\partial (4\pi M_{eff})} \right| \Delta (4\pi M_{eff}) \quad (13)$$

171 Finally, the last term which can contribute to the
172 linewidth is a residual frequency and angular indepen-
173 dent inhomogeneous linewidth that cannot be put in
174 other form.

175 The procedure used to determine the magnetic param-
176 eters is as follows: the anisotropy fields were determined
177 using the system of equations (5)-(8) applied at high sym-
178 metry directions (along easy/hard axes) together with
179 the corresponding measured resonance fields (fixed fre-
180 quency) at a fixed g -factor. Afterwards, the polar and
181 azimuthal angular dependence of the resonance field was
182 fitted with the same equations and the equilibrium con-
183 dition of the free energy allowing for a variable g -factor
184 as parameter. The iteration was repeated several times
185 until a good fit was obtained. This analysis yields the
186 g -factor, the anisotropy constants and the magnetization
187 direction θ . These values serve in the angular variation
188 of the linewidth which allows the evaluation of α , Γ and
189 the inhomogeneous contribution.

190 IV. RESULTS AND DISCUSSION

191 In this section, experimental results of C-doped
192 Mn_5Ge_3 thin films investigated by ferromagnetic reso-
193 nance and SQUID magnetometry are presented. Using
194 samples with different carbon content, we determined the
195 magnetic anisotropy energy, the g -factor, magnetization
196 and magnetic relaxation parameters.

A. Magnetic anisotropy

198 To determine the magnetic energy anisotropy (in ab-
199 solute units), FMR measurements were carried out at a
200 frequency of 9.4GHz. The FMR spectra were recorded
201 as a function of the polar and azimuthal angles of the
202 external magnetic field at different temperatures. The
203 saturation magnetization was determined from SQUID
204 measurements. In Fig. 2(d), the temperature dependence
205 of the magnetization up to 300K is shown for Mn_5Ge_3 ,
206 $\text{Mn}_5\text{Ge}_3\text{C}_{0.1}$ and $\text{Mn}_5\text{Ge}_3\text{C}_{0.2}$. The Curie temperature
207 was estimated from these curves by fitting with a Brill-
208 ouin function in reduced units. The full line correspond
209 to a fit with $B_{1.5}$ and the dotted line to a fit with B_1 .
210 The estimated values of T_c are 315K, 345K and 450K.
211 The error bars correspond to $\pm 10\text{K}$ for Mn_5Ge_3 and
212 $\text{Mn}_5\text{Ge}_3\text{C}_{0.1}$ as the experimental points cover a larger
213 temperature range and superpose closely with $B_{1.5}$. The
214 experimental points for $\text{Mn}_5\text{Ge}_3\text{C}_{0.2}$ cover only a small
215 part of the temperature range and the error bars are es-
216 timated to be of $\pm 30\text{K}$.

217 The out-of-plane angular variation for the reso-
218 nance field H_r is shown in Fig. 2(a)-(c) for Mn_5Ge_3 ,

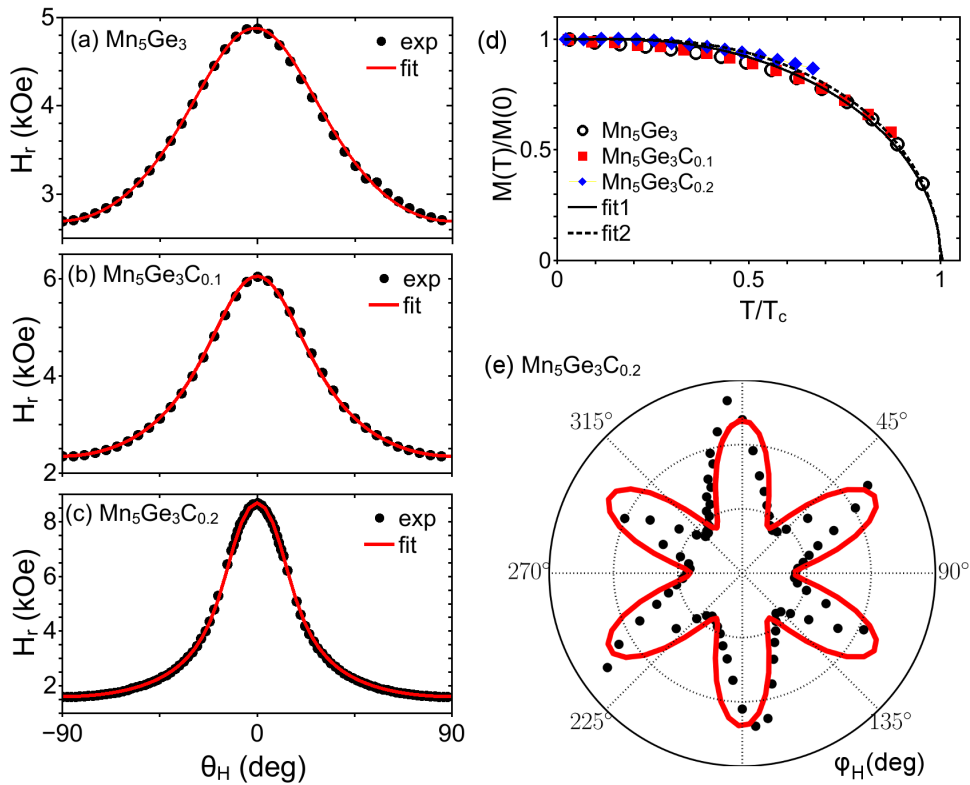


FIG. 2. (Color online) Out-of-plane angular variation of the resonance field at 300K for (a) Mn_5Ge_3 , (b) $\text{Mn}_5\text{Ge}_3\text{C}_{0.1}$, (c) $\text{Mn}_5\text{Ge}_3\text{C}_{0.2}$. The temperature dependence of the magnetization is shown in (d) in normalized coordinates. The full and dotted lines correspond to fits with a Brillouin function. The estimated T_c s are 315K, 345K and 450K. (e) In-plane angular dependence of the resonance field for $\text{Mn}_5\text{Ge}_3\text{C}_{0.2}$ at room temperature. The distance between dotted circles is 1 Oe. The line represents a fit with Eq.(3).

219 $\text{Mn}_5\text{Ge}_3\text{C}_{0.1}$ and $\text{Mn}_5\text{Ge}_3\text{C}_{0.2}$ at room temperature. The
 220 $H_r(\theta_H)$ indicate an easy axis along $H \parallel [100]$ (in-plane)
 221 with a minimum resonance field of 1.6kOe, 2.3kOe and
 222 2.7kOe for $\text{Mn}_5\text{Ge}_3\text{C}_{0.2}$, $\text{Mn}_5\text{Ge}_3\text{C}_{0.1}$ and Mn_5Ge_3
 223 respectively. The hard axis is perpendicular to plane ([001]
 224 direction) and has the highest H_r of 8.6kOe, 6kOe and
 225 5kOe. The azimuthal angular dependence of the resonance
 226 field for $\text{Mn}_5\text{Ge}_3\text{C}_{0.2}$, recorded also at 300K is
 227 shown in Fig. 2(e). The sixfold (hexagonal) symmetry in
 228 the azimuthal angular dependence indicates that an in-
 229 plane hexagonal anisotropy exists with easy axes along
 230 the [100] direction of the film. The experimental FMR
 231 data of out-of-plane and in-plane dependence of the res-
 232 onance field can be well simulated with Eq.(2) and the
 233 anisotropy fields can be extracted. The anisotropy con-
 234 stants can be found in absolute units by using the sample
 235 magnetization determined from SQUID measurements.

236 The resulting anisotropy constants are summarized
 237 in Table I along with the g -factor at several tempera-
 238 tures. The positive sign of K_2 indicates that this term
 239 favors an out-of-plane easy axis of magnetization while
 240 the shape anisotropy dominates²⁴. In the very thin film
 241 limit, K_2 could overcome the shape anisotropy result-
 242 ing in an out-of-plane anisotropy axis. The different K_i
 243 have a different temperature dependence. For Mn_5Ge_3

244 and $\text{Mn}_5\text{Ge}_3\text{C}_{0.1}$, the sixfold in-plane symmetry is to
 245 low to be extracted, therefore only the K_2 and K_4
 246 constants were determined from the angular measurements.
 247 K_2 is positive for Mn_5Ge_3 and C-doped Mn_5Ge_3 at all
 248 temperatures and increases at low temperature. K_4 de-
 249 creases (increases in absolute values) for Mn_5Ge_3 , but
 250 for the C-doped compounds has a minimum or a max-
 251 imum at an intermediate temperature. The sixfold in-
 252 plane anisotropy in $\text{Mn}_5\text{Ge}_3\text{C}_{0.2}$ increases at 250K from
 253 the room temperature value, while at lower temperature
 254 becomes to small or a transition to a fourfold in-plane
 255 anisotropy arises as will be inferred from the linewidth
 256 temperature dependence discussed in the next section.

257 The g -factor can be estimated from the angular de-
 258 pendence of the resonance field. Its value indicates the
 259 influence of the orbital contribution to the total magnetic
 260 moment. The ratio of the orbital to the spin magnetic
 261 moment can be inferred from the Kittel formula and is
 262 equal to the deviation of the g -factor from the free elec-
 263 tron value. The value of the g -factor for Mn_5Ge_3 and
 264 $\text{Mn}_5\text{Ge}_3\text{C}_{0.1}$ is 2.0005, while for $\text{Mn}_5\text{Ge}_3\text{C}_{0.2}$ this value
 265 increases to 2.0291 meaning an increased orbital con-
 266 tribution with Carbon doping (1.5% of the spin magnetic
 267 moment).

B. Magnetic relaxation

268

269 The linewidth of the resonant signal ΔH_r is directly related to the magnetic and structural quality of the films and provide information about the different relaxation channels in magnetic damping. In Fig. 3, the temperature dependence of the FMR linewidth is shown for the perpendicular to plane direction ($\theta_H = 0^\circ$) for Mn_5Ge_3 and C-doped Mn_5Ge_3 . A shallow minimum is observed for all three compounds around 200K and a sharp peak close to T_c . At lower temperature, the FMR linewidth increases and saturates for Mn_5Ge_3 (measured to 6K). The minimum in the linewidth seems not related with the C-doping. It occurs around the same absolute value of temperature and could be related with a small in-plane transition to a fourfold anisotropy from sixfold anisotropy (tetragonal distortion) or to a constriction by the substrate. The increase of linewidth at low temperature was explained as an inhomogeneous broadening due to the increase of the anisotropy constants (K_2) with decreasing temperature¹⁶.

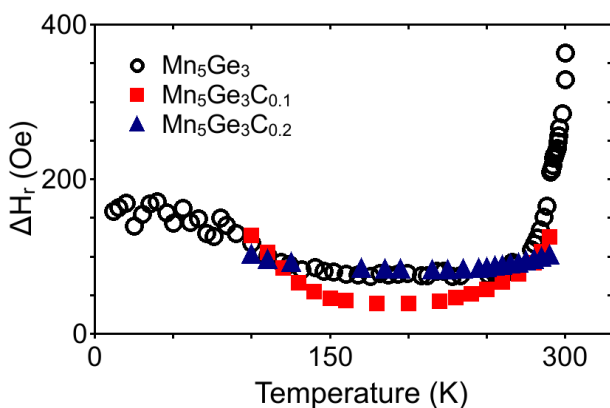


FIG. 3. (Color online) Temperature variation of the resonance linewidth for Mn_5Ge_3 , $\text{Mn}_5\text{Ge}_3\text{C}_{0.1}$ and $\text{Mn}_5\text{Ge}_3\text{C}_{0.2}$.

288 Fig. 4 and Fig. 5(a) show the out-of-plane variation of the FMR linewidth for the C-doped Mn_5Ge_3 compared to the pure Mn_5Ge_3 at room and low temperatures. The shape of the curves shows the characteristic dependence for thin films with a maximum of the linewidth at intermediate angles. Our films have an in-plane easy axis at all temperatures, therefore the magnetization lags behind the applied field when the field is rotated out of the plane. The peak in the linewidth occurs for θ_H between 20° at room temperature and 10° at low temperature, corresponding to the largest interval between \mathbf{M} and \mathbf{H} . From the theoretical fits of the data (solid lines), the relaxation parameters are extracted and listed in Table II.

301 For all three compounds, the perpendicular to plane linewidth is always smaller than the in-plane one indicating the presence of two-magnon scattering and other extrinsic contributions in the samples. The intrinsic damping cannot explain the out-of-plane shape of the linewidth. The estimated intrinsic damping is considered

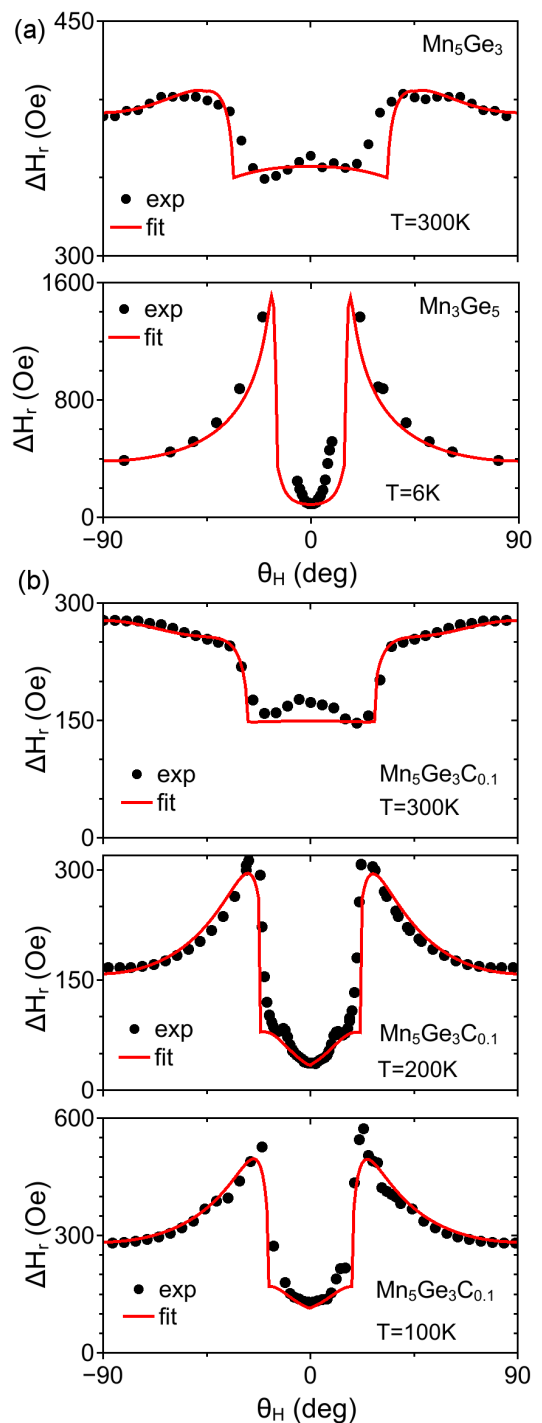


FIG. 4. (Color online) Out-of-plane angular dependence of the resonance linewidth for Mn_5Ge_3 (a) and $\text{Mn}_5\text{Ge}_3\text{C}_{0.1}$ (b) at different temperatures. The lines represent fits with intrinsic and extrinsic contributions.

307 isotropic and independent of temperature. We prefer using the dimensionless parameter α which varies between 308 0.005 and 0.01 over the Gilbert damping parameter G 309 given by $\alpha = G/\gamma M$ as the latter will imply a tempera- 310 ture dependence. The Gilbert damping represents the 311

312 decay of magnetization by direct viscous dissipation to
 313 the lattice as it is introduced in the Landau-Lifschitz-
 314 Gilbert equation¹⁸. The spin-orbit coupling is assumed
 315 to be at the origin of spin-lattice relaxation in ferro-
 316 magnets. *Ab-initio* calculations that include the spin-
 317 orbit coupling explicitly show a weak dependence of α
 318 with temperature in a large range of temperatures^{25,26}.
 319 Two different mechanisms contribute to the temperature
 320 dependence²⁷, one conductivity-like and one resistivity-
 321 like with a transition between the two at intermediate
 322 temperature. Sometimes these two contributions have an
 323 equal influence on the damping. We estimated the value
 324 of α for each compound by fitting the out-of-plane angu-
 325 lar dependence of ΔH_r at a temperature corresponding
 326 to the minimum of the curves in Fig. 3 (around 200K).
 327 For this specific temperature, the estimation correspond
 328 to the maximum possible value of α considering small in-
 329 homogeneous broadening (ΔH_{int} and ΔH_{inh}). Although
 330 we consider a constant α , as it is observed from Table II,
 331 at room and low temperature the linewidth (and corre-
 332 spondingly the inhomogeneous residual field) increases
 333 for $\text{Mn}_5\text{Ge}_3\text{C}_{0.1}$ which could be explained by an increase
 334 of α at least at low temperature. The room tempera-
 335 ture increasing in the linewidth is usually explained as a
 336 breakdown of the uniform precession due to thermal ex-
 337 citations. The increasing of the linewidth at low temper-
 338 ature is smaller for Mn_5Ge_3 and $\text{Mn}_5\text{Ge}_3\text{C}_{0.2}$ in the 100-
 339 300K temperature range being compatible with a con-
 340 stant α as considered.

341 The second relaxation mode that influence the FMR
 342 linewidth is the two magnon scattering. The uni-
 343 form mode can couple with degenerate spin-wave modes
 344 due to fluctuations in the local effective field that can
 345 arise from surface defects, scattering centers, fluctua-
 346 tion in the anisotropy from grain to grain or other
 347 inhomogeneities^{20,22}. The two magnon scattering rate
 348 Γ depends on the angle θ_H (out-of-plane geometry) and
 349 on the resonance field H_{res} . A detailed analysis based
 350 on the effect of the defects on the response functions of
 351 thin films was performed in Refs.21 and 28 for the case
 352 when the magnetization is tipped out-of-plane. We con-
 353 sider here the same type of angular dependence of Γ as in
 354 Ref.28 (see Eq.8). Γ depends on the nature and shape of
 355 the defects that activate the scattering mechanism. The
 356 values for the Mn_5Ge_3 compounds, extracted from the
 357 fitting of the linewidth curves, are shown in Table II as
 358 a function of temperature. From the calculated value
 359 $\Gamma_{2mag}=8H_K b^2 p/\pi D$, the exchange spin-wave stiffness D
 360 can be inferred if details of the defects as the covered frac-
 361 tion of the surface p or the effective height b are known
 362 (H_K the anisotropy field). Atomic force microscopy mea-
 363 surements were performed on the samples, from which
 364 the rms surface roughness was determined: for Mn_5Ge_3
 365 the surface roughness was of the order of 1.5-2nm, while
 366 for $\text{Mn}_5\text{Ge}_3\text{C}_x$ was of the order of 1nm. Therefore, at
 367 room temperature, the spin-wave stiffness was estimated
 368 as $0.12 \times 10^{-8} \text{G cm}^2$ for Mn_5Ge_3 , $0.16 \times 10^{-8} \text{G cm}^2$ for
 369 $\text{Mn}_5\text{Ge}_3\text{C}_{0.1}$ and $0.39 \times 10^{-8} \text{G cm}^2$ for $\text{Mn}_5\text{Ge}_3\text{C}_{0.2}$ con-

370 sidering a defect ratio of 50%. These values are only esti-
 371 mates as a precise identification of the defects is difficult
 372 to obtain.

373 As observed from Table II, the other extrinsic contri-
 374 butions to the linewidth have only a small impact on the
 375 fitted curves. The mosaicity is very small, inferior to
 376 0.1° , being almost negligible testimony of the good qual-
 377 ity of our samples. Also the inhomogeneity of the internal
 378 fields is almost negligible in the majority of cases, only
 379 for $\text{Mn}_5\text{Ge}_3\text{C}_{0.1}$ at room temperature it seems to have
 380 a larger influence. The higher values of H_{int} are needed
 381 to explain the small peak observed around $\theta_H = 0^\circ$ for
 382 both Mn_5Ge_3 and $\text{Mn}_5\text{Ge}_3\text{C}_{0.1}$ and for the increase of
 383 the linewidth at intermediate angles until $\theta_H = 90^\circ$ for
 384 $\text{Mn}_5\text{Ge}_3\text{C}_{0.1}$ at room temperature. The values of the
 385 residual inhomogeneous contribution are generally small,
 386 the larger values can also be attributed to a temperature
 387 dependent intrinsic contribution as discussed above.

388 We now discuss the case of $\text{Mn}_5\text{Ge}_3\text{C}_{0.2}$ for which both
 389 out-of-plane and in-plane data was fitted as shown in
 390 Fig. 5. The panel (a) show the out-of-plane dependence
 391 of the FMR linewidth. The 300K and 250K data are well
 392 fitted close to $\theta_H = 0^\circ$ and at larger angles but not at the
 393 peaks that correspond to the largest interval between \mathbf{M}
 394 and \mathbf{H} (critical angle). The dashed line at $T=300\text{K}$ corre-
 395 sponds to a fit with the parameters indicated in Table II
 396 and $\Delta\theta_H = 0.05^\circ$, while the full line to a fit with $\Delta\theta_H$
 397 $= 0.2^\circ$. Although increasing the mosaicity contribution
 398 fits better the peaks, the fitted curve becomes V-shaped
 399 between the peaks in total contradiction with the data.
 400 We believe that the mosaicity is small (0.05°) and the
 401 discrepancy at the critical angle at 300K is due to some
 402 other effect (the FMR line being strongly distorted at this
 403 angle). We also tried to fit the 300K curve introducing in-
 404 plane second and fourth order anisotropy constants ($K_{2\parallel}$
 405 and $K_{4\parallel}$) without a better result (not shown). The low
 406 temperature curves are nicely fitted with the presented
 407 model for all angles.

408 For the in-plane dependence of ΔH_r , the only contri-
 409 butions that were considered were from the isotropic in-
 410 trinsic damping and the two-magnon contribution which
 411 was expressed as follows^{19,20,28}:

$$412 \Delta H_{2mag} = \frac{\sum_i \Gamma_i f(\varphi_i)}{\Psi} \arcsin \left(\sqrt{\frac{\sqrt{\omega_r^2 + (\omega_0/2)^2} - \omega_0/2}{\sqrt{\omega_r^2 + (\omega_0/2)^2} + \omega_0/2}} \right) \quad (14)$$

413 with $\omega_0 = \gamma M_{eff}$ and $\Gamma_i f(\varphi_i)$ characterize the
 414 anisotropy of the two-magnon scattering along different
 415 crystallographic in-plane directions. At 300K and 250K
 416 (Fig. 5(b)), the FMR linewidth has the same six-fold sym-
 417 metry as the angular dependence of H_r (Fig. 2(e)). If the
 418 scattering centers are given by lattice defects (disloca-
 419 tion lines), the azimuthal dependence should reflect the
 420 lattice symmetry^{19,29}. The angular dependence of the
 421 scattering was fitted with $\Gamma_i f(\varphi_i) = \Gamma_0 + \Gamma_2 \cos^2(\varphi -$
 422 $\varphi_2) + \Gamma_6 \cos 6(\varphi - \varphi_6)$ at 250K and 300K and with
 $\Gamma_i f(\varphi_i) = \Gamma_0 + \Gamma_2 \cos^2(\varphi - \varphi_2) + \Gamma_4 \cos 4(\varphi - \varphi_4)$ at 150K

and 100K. The parameters Γ_2 and Γ_4 are phenomenologically introduced to account for the observed angular variation. Γ_6 is expected from the sixfold symmetry. The in-plane anisotropies are very small as observed from their values in Table III, therefore $\varphi_M \approx \varphi_H$ and the dragging function is very close to one and neglected. A change of symmetry of the scattering seems to take place around 200K corresponding to the minimum in Fig. 3. At lower temperature a superposition of twofold and fourfold symmetry dominates the angular dependence of the in-plane linewidth. This cannot be related only to crystalline defects as the azimuthal dependence of the resonance field show a small highly distorted uniaxial anisotropy along the 45° direction (not shown). More experimental measurements are needed to elucidate the linewidth transition at 200K.

V. CONCLUSION

Mn_5Ge_3 and $\text{Mn}_5\text{Ge}_3\text{C}_x$ films with 12nm thickness were grown by reactive deposition epitaxy on Ge(111) substrates. Detailed FMR measurements were performed on the samples at different temperatures. Both

Mn_5Ge_3 and C-doped Mn_5Ge_3 show perpendicular uniaxial magneto-crystalline anisotropy and an in-plane easy axis of magnetization due to the large shape anisotropy. The small linewidth of the films are a proof of the good quality of all the samples. From the angular dependence of the resonance field and of the linewidth, the anisotropy fields, g -factor and magnetic relaxation parameters are obtained. The contributions to the broadening of the FMR linewidth come primarily from the intrinsic Gilbert damping and two-magnon scattering. A transition from the six-fold to two-fold plus fourfold in-plane anisotropy was determined around 200K for $\text{Mn}_5\text{Ge}_3\text{C}_{0.2}$ that corresponds to the minimum in the temperature dependence of the out-of-plane linewidth.

ACKNOWLEDGEMENTS

This work has been carried out thanks to the support of the A*MIDEX project (No. ANR-11-IDEX-0001-02) funded by the "Investissements d'Avenir" French Government program, managed by the French National Research Agency (ANR). We also want to thank the interdisciplinary French EPR network RENARD (CNRS - FR3443).

-
- ¹ I. Zutic, J. Fabian, and S. D. Sarma, Rev. Mod. Phys. **76**, 323 (2004).
² D. D. Awschalom and M. E. Flatté, Nature Phys. **3**, 153 (2007).
³ G. Schmidt, D. Ferrand, L. W. Molenkamp, A. T. Filip, and B. J. van Wees, Phys. Rev. B **62**, R4790 (2000).
⁴ C. Zeng, S. C. Erwin, L. C. Feldman, A. P. Li, R. Jin, Y. Song, J. R. Thompson and H. H. Weitering, App. Phys. Lett. **83**, 5002 (2003).
⁵ M. Gajdzik, C. Sürgers, M. Kelemen, and H. v. Löhneysen, J. Magn. Magn. Mater. **221**, 248 (2000).
⁶ R. P. Panguluri, C. Zeng, H. H. Weitering, J. M. Sullivan, S. C. Erwin, and B. Nadgorny, Phys. Status Solidi B **242**, R67 (2005).
⁷ S. Picozzi, A. Continenza, and A. J. Freeman, Phys. Rev. B **70**, 235205 (2004).
⁸ C. Sürgers, G. Fischer, P. Winkel, and H. v. Löhneysen, Phys. Rev. B **90**, 104421 (2014).
⁹ I. Slipukhina, E. Arras, P. Mavropoulos, and P. Pochet, Appl. Phys. Lett. **94**, 192505 (2009).
¹⁰ S. Olive-Mendez, A. Spiesser, L.A. Michez, V. Le Thanh, A. Glachant, J. Derrien, T. Devillers, A. Barski, M. Jamet, Thin Solid Films **517**, 191 (2008).
¹¹ Matthieu Petit, Lisa Michez, Charles-Emmanuel Dutoit, Sylvain Bertaina, Voicu O. Dolocan, Vasile Heresanu, and Vinh Le Thanh, *submitted to Thin Solid Films* (2015).
¹² L. Simon, M. Stoffel, P. Sonnet, L. Kubler, L. Stauffer, A. Selloni, A. De Vita, R. Car, C. Pirri, G. Garreau, D. Aubel, and J. L. Bischoff, Phys. Rev. B **64**, 035306 (2001).
¹³ C. Zeng, W. Zhu, S. C. Erwin, Z. Zhang, and H. H. Weitering, Phys. Rev. B **70**, 205340 (2004).
¹⁴ M. Farle, Rep. Prog. Phys. **61**, 755 (1998).
¹⁵ C. Chappert, K. L. Dang, P. Beauvillain, H. Hurdequint, and D. Renard, Phys. Rev. B **34**, 3192 (1986).
¹⁶ W. Platow, A. N. Anisimov, G. L. Dunifer, M. Farle, and K. Baberschke, Phys. Rev. B **58**, 5611 (1998).
¹⁷ S. Mizukami, Y. Ando, and T. Miyazaki, Jpn. J. Appl. Phys. **40**, 580 (2001).
¹⁸ T. L. Gilbert, IEEE Trans. Magn. **40**, 3443 (2004).
¹⁹ K. Zakeri, J. Lindner, I. Barsukov, R. Meckenstock, M. Farle, U. von Hörsten, H. Wende, W. Keune, J. Rucker, S. S. Kalarickal, K. Lenz, W. Kuch, K. Baberschke, and Z. Frait, Phys. Rev. B **76**, 104416 (2007).
²⁰ R. Arias and D. L. Mills, Phys. Rev. B **60**, 7395 (1999).
²¹ P. Landeros, R. E. Arias, and D. L. Mills, Phys. Rev. B **77**, 214405 (2008).
²² R. D. McMichael, D. J. Twisselmann, and A. Kunz, Phys. Rev. Lett. **90**, 227601 (2003).
²³ S. S. Kalarickal, P. Krivosik, J. Das, K. S. Kim, and C. E. Patton, Phys. Rev. B **77**, 054427 (2008).
²⁴ A. Truong, A. O. Watanabe, T. Sekiguchi, P. A. Morte-mousque, T. Sato, K. Ando, and K. M. Itoh, Phys. Rev. B **90**, 224415 (2014).
²⁵ K. Gilmore, Y. U. Idzerda, and M. D. Stiles, Phys. Rev. Lett. **99**, 027204 (2007).
²⁶ H. Ebert, S. Mankovsky, D. Ködderitzsch, and P. J. Kelly, Phys. Rev. Lett. **107**, 066603 (2011).
²⁷ B. Heinrich, *Ultrathin Magnetic Structures III* (Springer, New York, 2005).
²⁸ J. Lindner, I. Barsukov, C. Raeder, C. Hassel, O. Posth, R. Meckenstock, P. Landeros, and D. L. Mills, Phys. Rev. B **80**, 224421 (2009).
²⁹ G. Woltersdorf and B. Heinrich, Phys. Rev. B **69**, 184417 (2004).

TABLE I. Magnetic parameters for Mn_5Ge_3 , $\text{Mn}_5\text{Ge}_3\text{C}_{0.1}$ and $\text{Mn}_5\text{Ge}_3\text{C}_{0.2}$ at different temperatures obtained from the FMR.

Sample	T(K)	$4\pi M_{eff}$ (kOe)	K_2 (erg/cm ³)	K_4 (erg/cm ³)	$K_{6\parallel}$ (erg/cm ³)	$\gamma/2\pi$ (GHz/kOe)
Mn_5Ge_3	300	1.5	3.7×10^5	2832.45		2.8
	250	4.3	9.95×10^5	682.68		2.8
	200	4.6	1.69×10^6	-1.19×10^5		2.8
	6	5.4	3.95×10^6	-9.84×10^5		2.8
$\text{Mn}_5\text{Ge}_3\text{C}_{0.1}$	300	2.6	1.65×10^6	3.85×10^4		2.8
	250	3.8	2.71×10^6	-1901		2.8
	200	4.4	3.37×10^6	-5131.37		2.8
	100	5.0	4.29×10^6	2.58×10^4		2.8
$\text{Mn}_5\text{Ge}_3\text{C}_{0.2}$	300	5.3	4.39×10^6	4.41×10^4	27.95	2.84
	250	5.8	4.78×10^6	5.53×10^4	134.17	2.84
	150	6.6	5.19×10^6	5.35×10^4		2.84
	100	7.0	5.28×10^6	4.61×10^4		2.84

TABLE II. Magnetic relaxation parameters for Mn_5Ge_3 , $\text{Mn}_5\text{Ge}_3\text{C}_{0.1}$ and $\text{Mn}_5\text{Ge}_3\text{C}_{0.2}$ at different temperatures determined from the out of plane angular variation of FMR.

Sample	T(K)	α	Γ_{2mag} (Oe)	$\Delta\theta_H$ (deg)	$\Delta(4\pi M_{eff})$ (Oe)	ΔH_{inh} (Oe)
Mn_5Ge_3	300	0.01	150	0.05	20	270
	6	0.01	600	0.1	10	10
$\text{Mn}_5\text{Ge}_3\text{C}_{0.1}$	300	0.005	210	0.05	80	80
	250	0.005	280	0.1	5	15
	200	0.005	320	0.1	5	5
	150	0.005	400	0.1	5	5
	100	0.005	430	0.1	5	80
$\text{Mn}_5\text{Ge}_3\text{C}_{0.2}$	300	0.01	220	0.05-0.2	10	5
	250	0.01	300	0.05	10	5
	150	0.01	500	0.05	10	5
	100	0.01	450	0.05	10	5

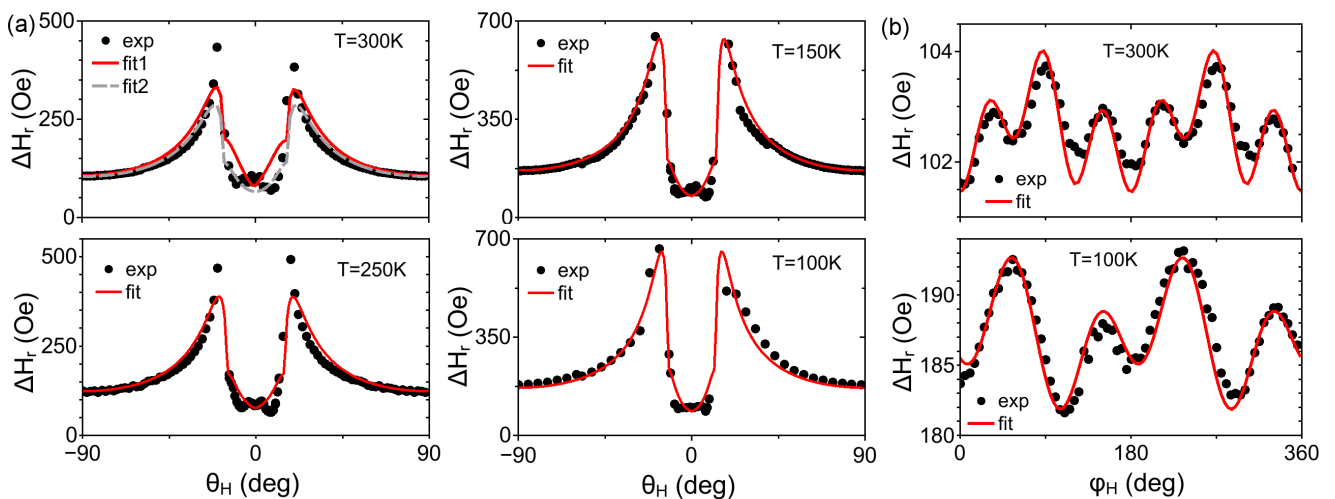
FIG. 5. (Color online) Out-of plane (a) and in-plane (b) angular dependence of the resonance linewidth for $\text{Mn}_5\text{Ge}_3\text{C}_{0.2}$ at different temperatures. The lines represent fits with intrinsic and extrinsic contributions.

TABLE III. Magnetic relaxation parameters for $\text{Mn}_5\text{Ge}_3\text{C}_{0.2}$ at different temperatures determined from the in-plane angular variation of FMR.

T(K)	$\Gamma_0(\text{Oe})$	$\Gamma_2(\text{Oe})$	$\Gamma_4(\text{Oe})$	$\Gamma_6(\text{Oe})$	φ_2	φ_4	φ_6
300	72.75	1.5		1.5	90		30
250	97.5	1.7		1.5	90		30
150	254.2	8.6	5.58		57	166	
100	291.4	12.4	8.68		57	167	